Supporting information for:

Synthesis of Lateral Size-Controlled Monolayer 1*H*-MoS_2@oleylamine as Supercapacitor Electrodes.

Nicky Savjani[†], Edward A. Lewis[‡], Mark A. Bissett[†], Jack R. Brent[‡], Robert A. W. Dryfe[†], Sarah J. Haigh[‡] and Paul O'Brien[†‡*]

[†] School of Chemistry and [‡] School of Materials, University of Manchester, Oxford Road, Manchester, M13 9PL, United Kingdom

1. Preliminary studies

1.1. Experimental

The chemicals molybdenum pentachloride, ammonium tetrathiomolybdate, sodium diethyl dithiocarbamate trihydrate, potassium ethylthioxanthate, hydrogen sulfide, phosphorous pentasulfide, methanol, ethanol, *p*-xylene, toluene, diethyl ether, THF, petroleum ether, chloroform, acetone, conc. hydrochloric acid and oleylamine were purchased from Sigma-Aldrich and all, except for oleylamine, were used as supplied. Oleylamine was dried before use by heating to 100 °C for 3 hours in a vacuum. The starting materials $[Mo_2O_3(S_2CNEt_2)_4]$ and $[Mo_2O_3(S_2COEt)_4]$ were prepared from known literature procedures.[1]

*1.1.1. Synthesis of $[Mo_2O_4(S_2CNEt_2)_2]$ (**Ia**)*

The procedure was modified from that described in literature.[2] In a nitrogen environment, $MoCl_5$ (5 g, 18 mmol) was carefully added to degassed H_2O (80 mL). The resulting solution was cooled to 5 °C before the removal of volatile gases (mainly HCl) by vacuum evacuation for 1 hour. After the reintroduction of nitrogen, the reaction was warmed to room temperature before a solution of $NaS_2CNEt_2 \cdot 3H_2O$

(4.1g, 18.2 mmol) in degassed methanol (225 mL) was added slowly and heated to reflux for 30 minutes. The resulting yellow precipitate was filtered, washed with a H_2O/EtOH solution (1:3, 2 × 75 mL) and dried in a vacuum overnight to give pure $[Mo_2O_4(S_2CNEt_2)_2]$ as a yellow powder (6.75 g, 12.2 mmol, 68 %). Anal. calcd for $C_{10}H_{20}Mo_2N_2O_4S_4$: C 21.74, H 3.65, N 5.07, S 23.17; found: C 21.97, H 3.51, N 5.05, S 23.30.

*1.1.2. Synthesis of $[Mo_2O_2S_2(S_2CNEt_2)_2]$ (**Ib**)*

The synthesis the title compound follows the procedure described in literature.[2] Yield - 1.01 g (1.73 mmol, 80 %) Anal. calcd for $C_{10}H_{20}Mo_2N_2O_2S_6$: C 20.57, H 3.45, N 3.45, S 32.85; found: C 20.69, H 3.48, N 4.74, S 32.85.

*1.1.3. Synthesis of $[Mo_2S_4(S_2CNEt_2)_2]$ (**Ic**)*

Complex $[Mo_2S_4(S_2CNEt_2)_2]$ was synthesised by two separate routes:

The first method was modified from that described in literature.[3] In a dry nitrogen environment, $[Mo_2O_4(S_2CNEt_2)_2]$ (3 g, 5.44 mmol) and P_4S_{10} (1.20 g, 2.72 mmol) were added to *p*-xylene (150 mL), before heating to reflux for 3 hours. The solution was then hot-filtered and the filtrate cooled to room temperature, yielding an orange-red microcrystalline powder. The powder was filtered and washed with cold toluene (2 × 30 mL) and dried in a vacuum overnight to give $[Mo_2S_4(S_2CNEt_2)_2]$ as an orange-red powder (1.31 g, 2.12 mmol, 39 %). Anal. calcd for $C_{10}H_{20}Mo_2N_2S_8$: C 19.50, H 3.27, N 4.55, S 41.53; found: C 19.33, H 3.11, N 4.61, S 41.09.

The second method follows the procedure described in literature.[4] Yield - 2.9 g (4.7 mmol, 61 %). Anal. calcd for $C_{10}H_{20}Mo_2N_2S_8$: C 19.50, H 3.27, N 4.55, S 41.53; found: C 19.61, H 3.31, N 4.53, S 41.98.

*1.1.4. Synthesis of $[Mo_2O_2S_2(S_2COEt)_2]$ (**IIb**)*

The synthesis of the title compound was modified from that described in literature.[1] In a dry nitrogen environment, a slow stream of H_2S was bubbled through a solution of $[Mo_2O_3(S_2COEt)_4]$ (5.6 g, 7.7 mmol) in dry chloroform (250 mL) for two hours. The reaction was sealed in the H_2S-rich environment and stirred overnight. After careful removal of volatile gases, the solvent was evaporated by vacuum to leave a dark brown powder. The by-products were removed from the solids by acetone extraction (2 × 100 mL) and filtration to give an orange powder. The powder was washed with acetone (2 × 50 mL) and dried in a vacuum to give pure $[Mo_2O_2S_2(S_2COEt)_2]$ as an orange powder (3.0 g, 5.6 mmol, 73 %). Anal. calcd. for $C_6H_{10}MoO_4S_6$: C 13.59, H 1.90, S 36.00; found: C 13.68, H 2.33, S 36.00.

*1.1.5. Synthesis of $[Mo_2S_4(S_2COEt)_2]$ (**IIc**)*

The procedure used was modified from that described in literature.[1] In a dry nitrogen environment, a slow stream of H_2S was bubbled through a solution of $[Mo_2O_3(S_2COEt)_4]$ (10 g, 13.8 mmol) in a toluene-ethanol solvent mixture (4:1, 250 mL) for two hours. The reaction was sealed in the H_2S-rich environment and stirred overnight. The dark-brown precipitate was filtered, washed with petroleum ether (3 × 100 mL) and dried in a vacuum to give pure $[Mo_2S_4(S_2COEt)_2]$ as a dark brown solid

(3.9 g, 7.0 mmol, 51 %). Anal. calcd. for $C_6H_{10}MoO_2S_8$: C 12.82, H 1.79, S 45.53; found: C 12.58, H 1.71, S 45.04.

1.1.6. 1H-MoS_2@Oleylamine synthesis by hot injection

In a typical synthesis, a 200 mg solution of the selected precursor in oleylamine (5 mL) was rapidly added to hot oleylamine (35 mL; reaction temperatures ranged from 200 to 325 °C) under stirring. The solution turned a black colour and drops in reaction temperatures of 10-30 °C was observed; the reaction was kept at the lower temperature after addition. 9 mL aliquots were taken at regular intervals and added to methanol (35 mL), resulting in a flocculant-like precipitate. The black precipitate was separated by centrifugation (4,000 rpm for 20 minutes) and the supernatant removed. The precipitate was washed by repeated dispersion into 40 mL methanol and centrifugation before 1*H*-MoS_2@oleylamine was finally dried in a vacuum for 16 hours.

1.2. Results and discussion

In determining the best suited precursor for the synthesis of 1*H*-MoS_2@oleylamine, a series of molybdenum(V) complexes that contain dithiocarbamate and xanthate ligands were synthesised following literature procedures (**Ia-c**, **IIb-c**; **Figure S1**). The precursors were deemed pure by elemental analyses and analytical data were in agreement with the corresponding references. The complexes were isolated as fine powders of various colours that were found to have little to no solubility in organic solvents (such as dichloromethane, THF and toluene), but were soluble in

oleylamine. It was found that cold storage (-30 °C) of the xanthate-containing complexes **IIb** and **IIc** was necessary to inhibit decomposition.

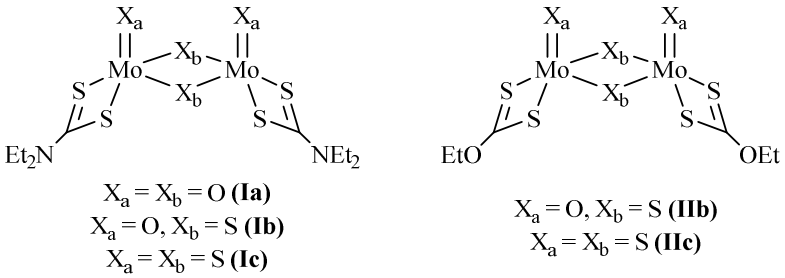

$X_a = X_b = O$ **(Ia)**
$X_a = O, X_b = S$ **(Ib)**
$X_a = X_b = S$ **(Ic)**

$X_a = O, X_b = S$ **(IIb)**
$X_a = X_b = S$ **(IIc)**

Figure S1. The $MoX_4(S_2CNEt_2)_2$ and $MoX_4(S_2COEt)_2$ complexes studied in this research.

TGA was used to follow the decomposition pathways of the complexes in an inert, nitrogen environment, comparing the effect of ligand variation within the precursors (**Figure S2**). Complex **Ia** decomposes in three steps from 231 to 374 °C. The thermogram of **Ib** shows a single, sharp decomposition step between 318 and 392 °C. Complex **IIb** decomposes in two steps between 99 and 406 °C, following a similar decomposition pathway seen in the molybdenum(V) complex $[Mo_2O_3(S_2COEt)_4]$.[5] The final weight of the residues of **Ia** (57.7 %), **Ib** (54.5 %) and **IIb** (61.3 %) are in close agreement to the predicted residual weights of two MoS_2 molecules (57.9, 54.8 and 60.4 %, respectively). The feature of the ethylxanthate ligand in **IIb** breaking down at a considerably lower temperature than its dithiocarbamate analogues **Ia** and **Ib** has been observed under similar conditions. [5, 6] The decomposition of the tetrasulfido-complexes **Ic** and **IIc** start at 107 and 177 °C, respectively, but mass losses were still observed after 10 minutes in the analytical

furnace at 1,000 °C. This is thought to occur as the result of the stability of the intermediates formed; in the cases of the ethylxanthate-containing complexes, it is thought that an [$MoXS_2$] intermediate is formed (where X corresponds to S or O, sourced from the initial [$Mo_2X_2S_2(S_2COEt)_2$] precursor). The [$MoOS_2$] intermediate from **IIb** is unstable, readily breaking down to MoS_2 whereas MoS_3, formed from **IIc**, is a metastable material which is known to require a lengthy annealing stage for reduction to MoS_2 to occur.[7] This assignment cannot currently be made with the Mo(S_2CNEt_2) complexes as the intermolecular sulfonation step inherent with this ligand system complicates the mechanism,[6] but assume a similar mechanistic step is prevalent.

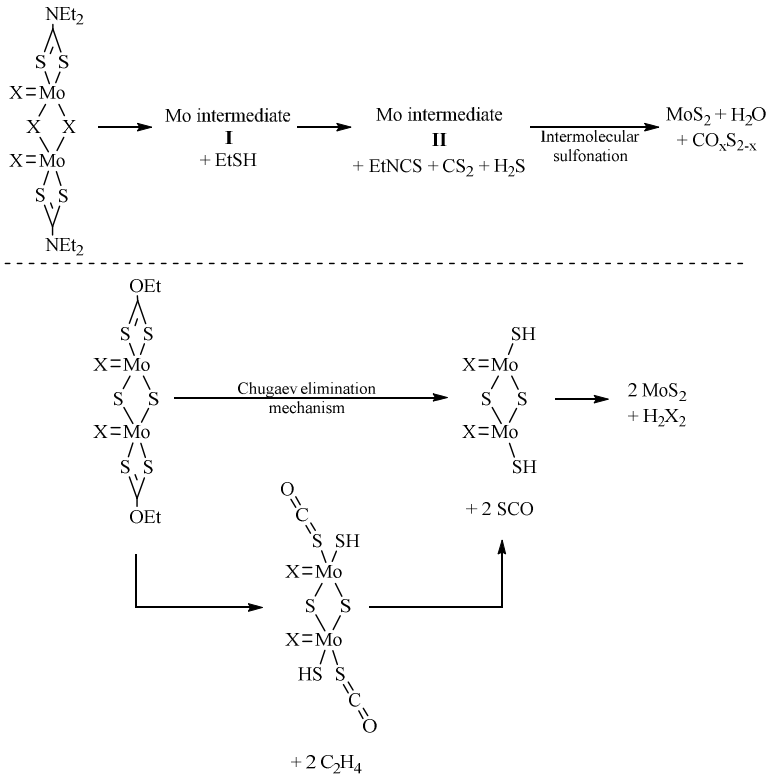

Scheme S1. The proposed decomposition pathways of the molybdenum(V) complexes (**Ia-c**, **IIb-c**) to MoS_2.

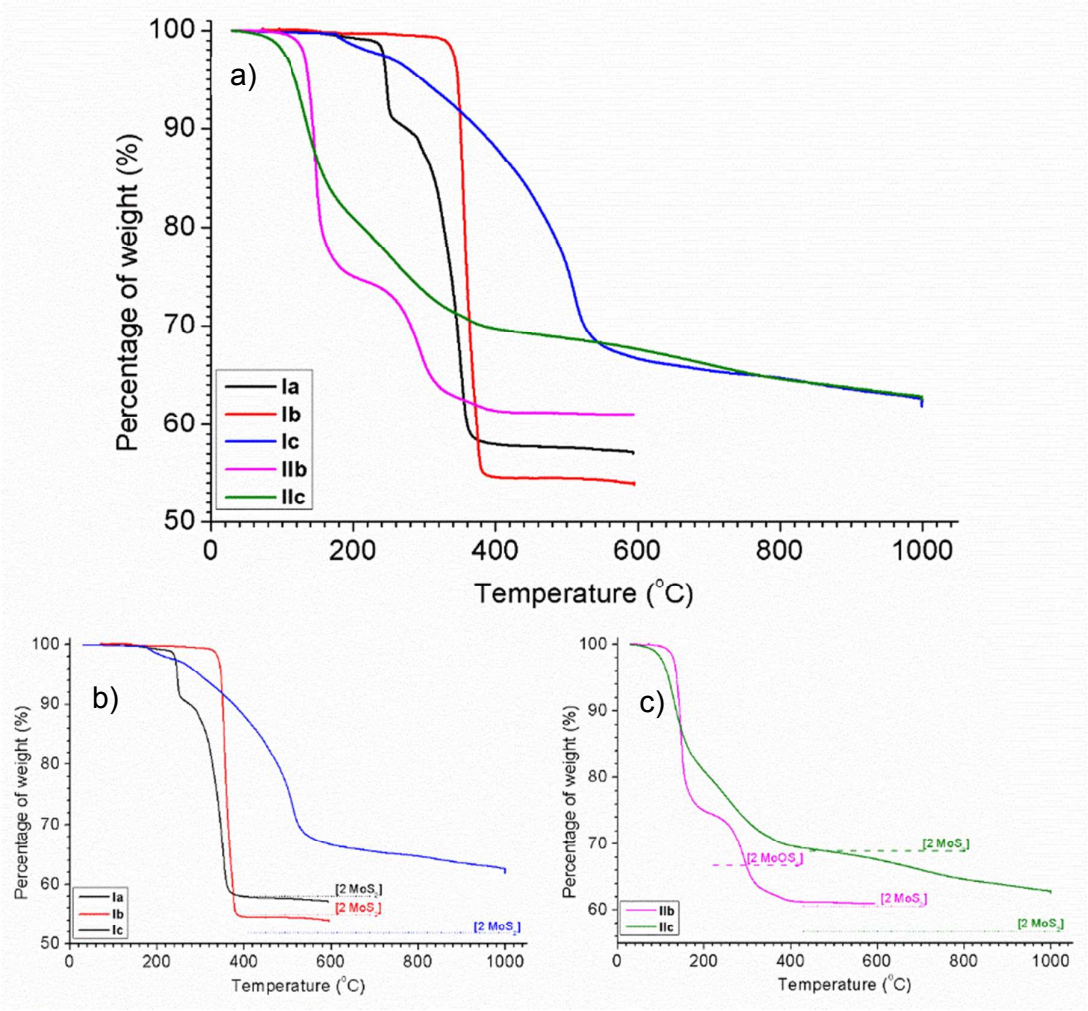

Figure S2. (a) Thermograms of the molybdenum(V) complexes of interest. The thermograms of (b) the Mo(diethyldithiocarbamate) and (c) Mo(ethylxanthate) (bottom right) complexes were separated for clarity, with calculated residues of proposed intermediates.

Initial hot injection reactions with the family of precursors were carried out at 200, 250 and 300 °C for 30 minutes. Basic analyses were carried out on the materials produced; the results are found in **Table S1**. A number of trends were observed: 1) The diethyldithiocarbamato-containing complexes did not break down effectively at

200 °C, resulting in a large amount of unreacted precursor remaining in the supernatant and a significantly smaller crop of 1*H*-MoS_2@oleylamine isolated. The ethylxanthate complexes, on the other hand, had completely decomposed within the 30 minutes. 2) The purity of the products from the hot injection of $[Mo_2O_2S_2(S_2COEt)_2]$ was up to 10 % higher than those obtained from the sulfur-rich $[Mo_2S_4(S_2COEt)_2]$, with the majority of the additional by-products arising from sulfur impurities on the surface of the material. 3) The purity of all 1*H*-MoS_2@olelyamine products have a significant reduction when the hot injections were carried out at 300 °C. 4) A similar reduction of the Raman bands separation with increasing injection temperature seen in the main article was observed here. Considering both the TGA and hot-injection data obtained, we chose $MoO_2S_2(S_2COEt)_2$ as the precursor for our detailed studies as it garnered MoS_2 at the temperatures as low as 200 °C.

Table S1. The summation of the data obtained for the precursor survey in the production of MoS_2@oleylamine by hot-injection thermolysis.

Reaction precursor	Reaction Temperature (°C)	Purity (%)	Raman bands separation (cm^{-1})
$Mo_2O_2S_2(S_2COEt)_2$ (**IIb**)	200	73	25
$Mo_2O_2S_2(S_2COEt)_2$ (**IIb**)	250	71	24
$Mo_2O_2S_2(S_2COEt)_2$ (**IIb**)	300	21	22
$Mo_2S_4(S_2COEt)_2$ (**IIc**)	200	65	27
$Mo_2S_4(S_2COEt)_2$ (**IIc**)	250	64	24
$Mo_2S_4(S_2COEt)_2$ (**IIc**)	300	22	22
$Mo_2O_4(S_2CNEt_2)_2$ (**Ia**)	200	76	24
$Mo_2O_4(S_2CNEt_2)_2$ (**Ia**)	250	75	25
$Mo_2O_4(S_2CNEt_2)_2$ (**Ia**)	300	16	22
$Mo_2O_2S_2(S_2CNEt_2)_2$ (**Ib**)	200	77	25
$Mo_2O_2S_2(S_2CNEt_2)_2$ (**Ib**)	250	75	25
$Mo_2O_2S_2(S_2CNEt_2)_2$ (**Ib**)	300	18	22
$Mo_2S_4(S_2CNEt_2)_2$ (**Ic**)	200	61	24
$Mo_2S_4(S_2CNEt_2)_2$ (**Ic**)	250	75	24
$Mo_2S_4(S_2CNEt_2)_2$ (**Ic**)	300	22	22

2. TEM images of the 1*H*-MoS_2@oleylamine observed at lower magnification.

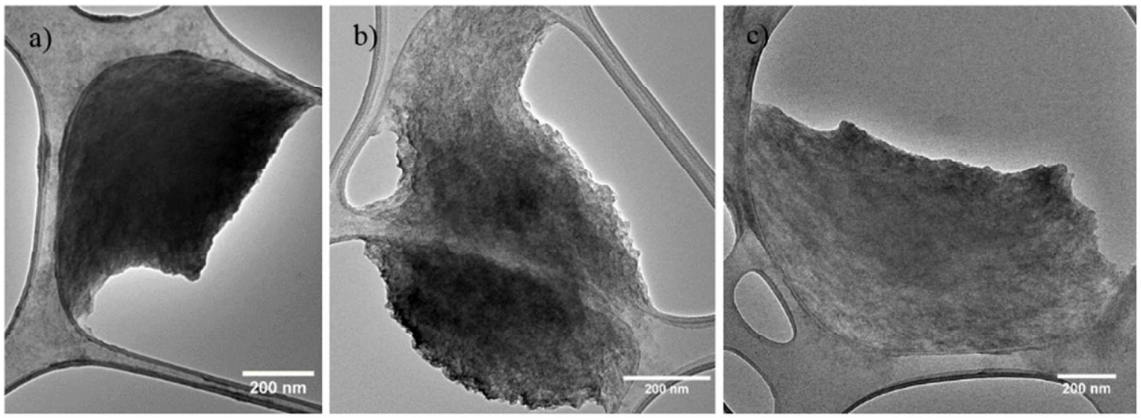

Figure S3. The typical nature of 1*H*-MoS_2@oleylamine flocculates on holey carbon grids. Images were obtained from 1*H*-MoS_2@oleylamine samples (a) 3, (b) 7 and (c) 15.

3. Determining the composition of 1*H*-MoS_2@oleylamine.

There are four stages of decomposition observed in all 1*H*-MoS_2@oleylamine samples by TGA, which have been described previously by Altavilla *et al* (see **Figure S4**).[8] We can both qualitatively and quantitatively assign the residual masses at the ends of each stage from the thermogram data: m_{T1} (at 360 °C) – 1*H*-MoS_2@oleylamine and physisorbed oleylamine, m_{T2} (at 475 °C) – 1*H*-MoS_2@oleylamine only and m_{T3} (at 580 °C) – MoO_3 only.

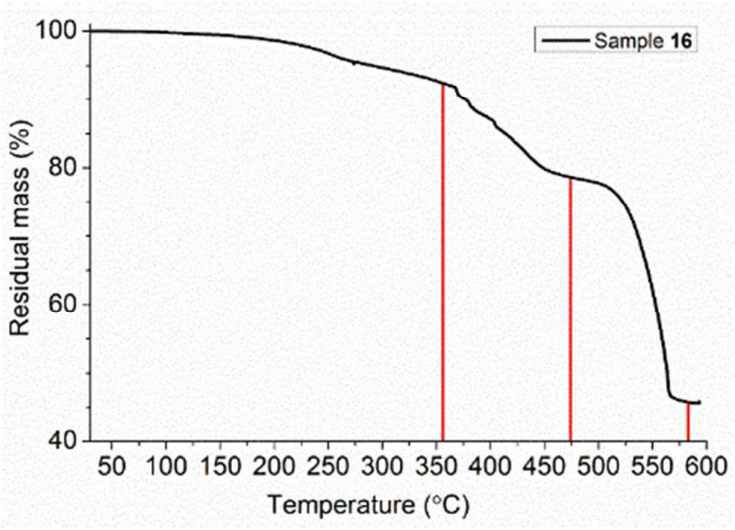

Figure S4. A representative thermogram for the decomposition of 1*H*-MoS_2@oleylamine (sample 16) in air. The temperatures that initiate the decomposition of the components within the materials are included in red.

The purity of the 1*H*-MoS_2@oleylamine material was simply found by **Equation S1**:

$$Purity\ of\ MoS_2@oleylamine\ (\%) = \frac{m_{T2}}{m_{T0}} \qquad \text{(S1)}$$

To calculate the composition of 1*H*-MoS_2@oleylamine, the relative masses of the components were determined (**Equation S2** and **S3**), before calculating the molar ratios of MoS_2 and chemisorbed oleylamine within the material (**Equation S4**-**8**):

$$mass\ of\ MoS_2: m_{\mathrm{MoS_2}} = m_{\mathrm{T3}} \times \frac{rmm_{\mathrm{MoS_2}}}{rmm_{\mathrm{MoO_3}}} = 1.111 m_{\mathrm{T3}} \quad \text{(S2)}$$

$$mass\ of\ chemisorbed\ oleylamine: m_{\mathrm{Oleylamine}} = m_{\mathrm{T2}} - m_{\mathrm{MoS_2}} \quad \text{(S3)}$$

$MoS_2@oleylamine\ ratio\ (MoS_2@oleylamine_x)$:

$$x = \frac{m_{\mathrm{oleylamine}}/rmm_{\mathrm{oleylamine}}}{m_{\mathrm{MoS_2}}/rmm_{\mathrm{MoS_2}}} \quad \text{(S4)}$$

$$x = 0.605 \frac{m_{\mathrm{Oleylamine}}}{m_{\mathrm{MoS_2}}} \quad \text{(S5)}$$

$$x = 0.605 \frac{\mathrm{m_{T2}} - 1.111 m_{\mathrm{T3}}}{1.111 m_{\mathrm{T3}}} \quad \text{(S6)}$$

$$x = 0.605 \frac{m_{\mathrm{T2}}}{1.111 m_{\mathrm{T3}}} - 0.605 \quad \text{(S7)}$$

$$x = 0.545 \frac{m_{\mathrm{T2}}}{m_{\mathrm{T3}}} - 0.605 \quad \text{(S8)}$$

4. Characterization data of the annealed MoS_2 films produced.

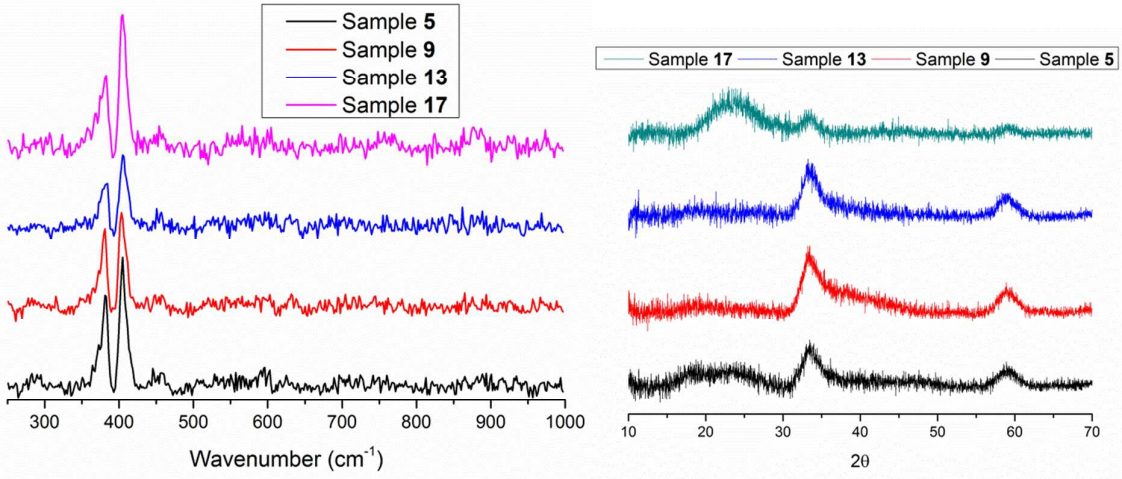

Figure S5. (a) Raman spectroscopy and thin film XRD patterns of the MoS_2 films produced after annealing at 500 °C in N_2. The characteristic patterns of MoS_2 are retained.

5. Electrochemical Impedance Spectroscopy.

Electrochemical impedance spectroscopy (EIS) was performed at a frequency range of 0.1 Hz to 100 kHz with a 10 mV (RMS) perturbation and 0 V dc bias. **Figure S6a** shows the Nyquist plot of the real (Z') and complex (Z'') impedance. The semi-circle at the high frequency region is due to ion diffusion while at low frequencies more capacitive behaviour dominates. From the Nyquist plot we can see that the equivalent series resistance (ESR) for the membrane is 1.39 Ω. The phase of the frequency response (**Figure S6b**) indicates that the dominant charge storage mechanism is not purely EDLC, but instead a combination of EDLC and surface based ion adsorption and intercalation, in agreement with our previous observations.[9] The initial decrease in phase with increasing frequency is attributed to the ion adsorption pseudocapacitance becoming dominant, however as the frequency continues to increase (100 – 10000 Hz) there is a small increase in the phase as the double-layer charge storage operates on a much faster time scale, and so is detected at higher frequencies. As the frequency increases further the phase decreases as expected due to diffusion limitations of the electrolyte ions.

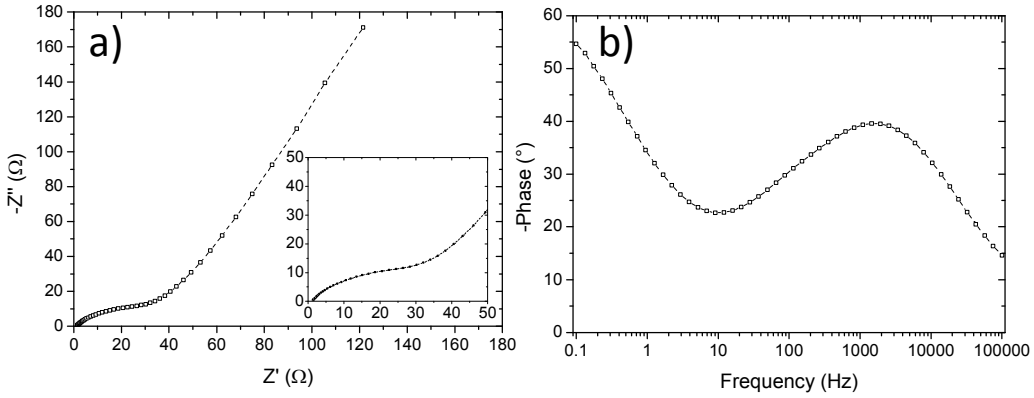

Figure S6. (a) Nyquist plot showing impedance at 0 V applied bias for frequencies ranging from 0.1 Hz to 100 kHz. Inset shows the high frequency region. (b) Bode plot showing the phase change with respect to frequency.

6. Cycling Stability.

Stability during repeated cycling is one of the key performance metrics for supercapacitor electrodes. Ideally, a supercapacitor electrode should exhibit a minimal decrease in capacitance with repeated use. Previously, it has been demonstrated that pure graphene supercapacitor electrodes can vary between almost no loss up to a 30% loss after 10,000 cycles.[10] Whilst pure MoS_2 electrodes have exhibited a 30% loss after only 200 cycles.[11] To determine the long term stability of the MoS_2/graphene composite coin cells used in this work repeated charge/discharge cycles were performed at a current density of 2.75 mA/cm^2 for 5000 cycles. The plot of the specific capacitance (%) as a function of cycle number is shown in **Figure S7**. We can see that with repeated cycling the specific capacitance increases from the initial value up to 240% after 3500 cycles before remaining constant thereafter. This increase in specific capacitance with repeated cycling has been observed previously in similar systems. The mechanism for this increased performance has been attributed to the continued adsorption and desorption of the electrolyte ions to the electrode surface, which leads to a partial re-exfoliation of the electrode membrane which is highly restacked during the filtration procedure, and is referred to in the literature as 'electro-activation'.[12-14] Indeed, we have previously reported very similar behavior when using solution exfoliated MoS_2/graphene composites in a similar electrode architecture.[9]

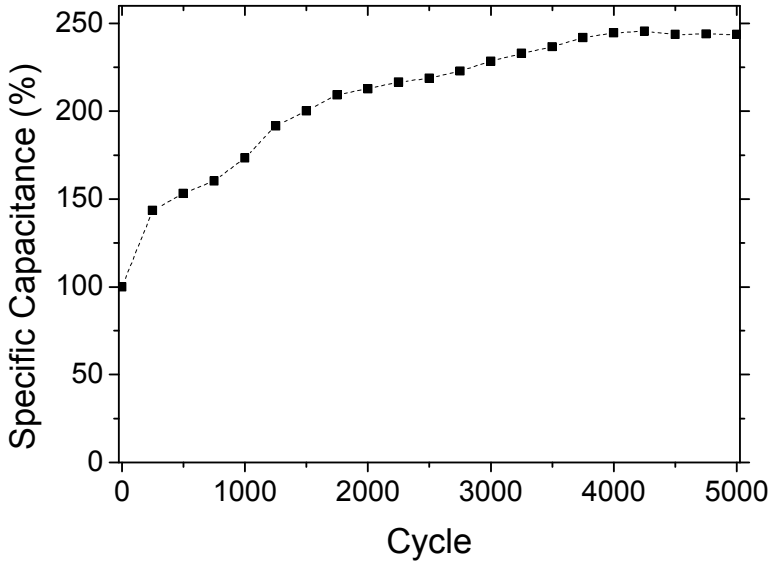

Figure S7. Cycling stability over 5000 charge/discharge cycles at a current density of 2.75 mA/cm^2 for the MoS_2/graphene composite.

7. Coulombic Efficiency.

The Coulombic efficiency of the composite coin cell was also calculated using the following formula; $\boldsymbol{\eta = \frac{Q_{discharge}}{Q_{charge}} \times 100}$. The galvanostatic charge/discharge curves from Figure 5c in the main text are shown in **Figure S8a** along with the plot of the Coulombic efficiency as a function of current density shown in **Figure S8b.** As the current density increases we observe an initial increase in the Coulombic efficiency; however, as the current density increases further there is a decrease due to the internal resistance of the cell. The highest value of η is only ~28%, and is lower than for an ideal supercapacitor due to the combination of charge storage mechanisms present. Specifically the large magnitude of the ion adsorption pseudocapacitance decreases the overall Coulombic efficiency.

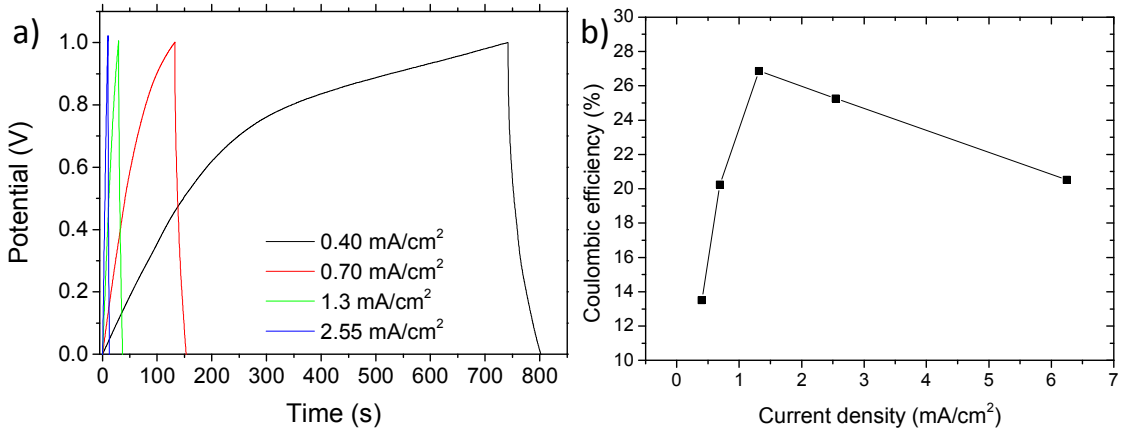

Figure S8. (a) Galvanostatic charge/discharge curves for the composite coin cell at varying current densities as shown. (b) Calculated Coulombic efficiencies with varying current density.

8. Ragone Plot.

Figure S9 shows the Ragone plot for the MoS_2/graphene composite coin cell. The energy density varies between 1 and 7 μWh/cm^2 while the power density varies between 1 and 3.5 mW/cm^2 for differing current densities. These values compare favorably against similar thin layer electrodes made from either pure graphene, carbon nanotubes or other inorganic TMDCs.[15, 16] To further increase these values it may be possible to use different organic electrolytes or ionic liquids to increase the potential window over which the cells can operate. As the present work uses aqueous electrolyte the potential window is limited to 1 V and as the energy scales with the square of the potential ($\boldsymbol{E = 1/2\, CV^2}$), by increasing this we can dramatically increase both the energy and power density.

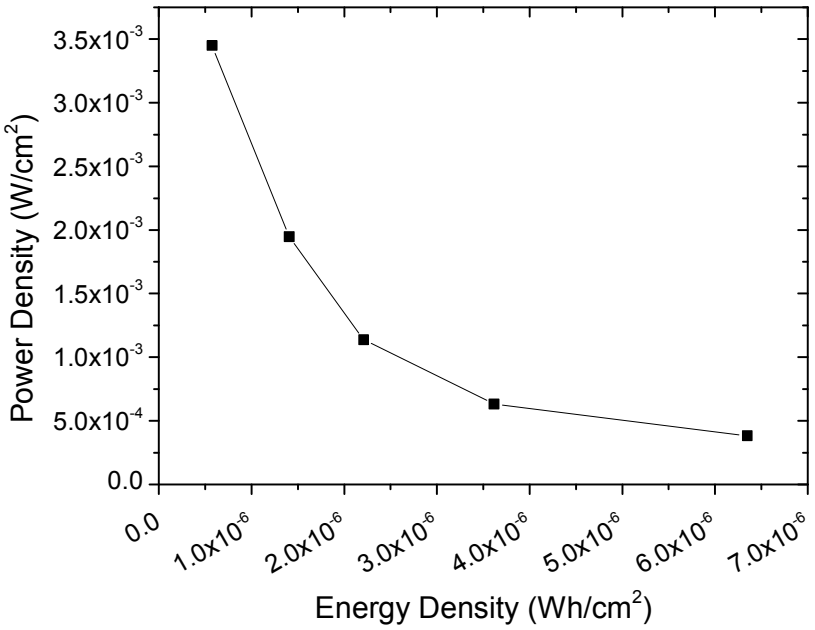

Figure S9. Ragone plot showing the energy and power densities at a range of current densities for the MoS_2/graphene composite coin cell.

References

1. Newton, W. E.; Corbin, J. L.; Bravard, D. C.; Searles, J. E.; McDonald, J. W., Preparation and Characterization of Two Series of Dimeric Molybdenum(V) N,N-dialkyldithiocarbamates. Their Interrelation and Chemistry as a Model for the Active Site of Nitrogenase. *Inorg. Chem.* **1974,** *13*, 1100-1104.
2. Schultz, F. A.; Ott, V. R.; Rolison, D. S.; Bravard, D. C.; McDonald, J. W.; Newton, W. E., Synthesis and Electrochemistry of Oxo- and Sulfido-Bridged Molybdenum(V) Complexes with 1,1-Dithiolate Ligands. *Inorg. Chem.* **1978,** *17*, 1758-1765.
3. Malik, M. A.; O'Brien, P.; Adeogun, A.; Helliwell, M.; Raftery, J., Synthesis and X-ray Single Crystal Structures of $[Mo(S_2CN^nBu_2)_4]$ and $[Mo_2S_4(S_2CN^nBu_2)_2].1/2H_2O$. *J. Coord. Chem.* **2008,** *61*, 79-84.
4. Coy Diaz, H.; Addou, R.; Batzill, M., Interface properties of CVD grown graphene transferred onto $MoS_2(0001)$. *Nanoscale* **2014,** *6*, 1071-1078.
5. Savjani, N.; Brent, J. R.; O'Brien, P., AACVD of Molybdenum Sulfide and Oxide Thin Films From Molybdenum(V)-based Single-source Precursors. *Chem. Vap. Depos.* **2015,** *21*, 71-77.
6. Mitchell, P. C. H., Oil-Soluble MO-S Compounds as Lubricant Additives. *Wear* **1984,** *100*, 281-300.
7. Weber, T.; Muijsers, J. C.; Niemantsverdriet, J. W., Structure of Amorphous MoS_3. *J. Phys. Chem.* **1995,** *99*, 9194-9200.
8. Altavilla, C.; Sarno, M.; Ciambelli, P., A Novel Wet Chemistry Approach for the Synthesis of Hybrid 2D Free-Floating Single or Multilayer Nanosheets of MS_2@oleylamine (M═Mo, W). *Chem. Mater.* **2011,** *23*, 3879-3885.
9. Bissett, M. A.; Kinloch, I. A.; Dryfe, R. A. W., Characterization of MoS_2–Graphene Composites for High-Performance Coin Cell Supercapacitors. *ACS Appl. Mater. Interfaces* **2015,** *7*, 17388-17398.
10. Xiong, G.; Meng, C.; Reifenberger, R. G.; Irazoqui, P. P.; Fisher, T. S., A Review of Graphene-Based Electrochemical Microsupercapacitors. *Electroanalysis* **2014,** *26*, 30-51.
11. Winchester, A.; Ghosh, S.; Feng, S.; Elias, A. L.; Mallouk, T.; Terrones, M.; Talapatra, S., Electrochemical Characterization of Liquid Phase Exfoliated Two-Dimensional Layers of Molybdenum Disulfide. *ACS Appl. Mater. Interfaces* **2014,** *6*, 2125-2130.
12. Beidaghi, M.; Wang, C., Micro-Supercapacitors Based on Interdigital Electrodes of Reduced Graphene Oxide and Carbon Nanotube Composites with Ultrahigh Power Handling Performance. *Adv. Funct. Mater.* **2012,** *22*, 4501-4510.
13. Cheng, Q.; Tang, J.; Ma, J.; Zhang, H.; Shinya, N.; Qin, L.-C., Graphene and carbon nanotube composite electrodes for supercapacitors with ultra-high energy density. *Phys. Chem. Chem. Phys.* **2011,** *13*, 17615-17624.
14. Cheng, Q.; Tang, J.; Ma, J.; Zhang, H.; Shinya, N.; Qin, L.-C., Graphene and nanostructured MnO_2 composite electrodes for supercapacitors. *Carbon* **2011,** *49*, 2917-2925.
15. Kou, L.; Huang, T.; Zheng, B.; Han, Y.; Zhao, X.; Gopalsamy, K.; Sun, H.; Gao, C., Coaxial Wet-Spun Yarn Supercapacitors for High-Energy Density and Safe Wearable Electronics. *Nature Commun.* **2014,** *5*, 3754.
16. Choi, C.; Kim, S. H.; Sim, H. J.; Lee, J. A.; Choi, A. Y.; Kim, Y. T.; Lepró, X.; Spinks, G. M.; Baughman, R. H.; Kim, S. J., Stretchable, Weavable Coiled Carbon

Nanotube/MnO_2/Polymer Fiber Solid-State Supercapacitors. *Sci. Rep.* **2015,** *5*, 9387.